minerals

MDPI

Article

Insights into Extinct Seafloor Massive Sulfide Mounds at the TAG, Mid-Atlantic Ridge

Berit Lehrmann [1,*], Iain J. Stobbs [2], Paul A.J. Lusty [3] and Bramley J. Murton [1]

[1] National Oceanography Centre, European Way, Southampton SO14 3ZH, UK; bramley.murton@noc.ac.uk
[2] National Oceanography Centre, University of Southampton Waterfront Campus, European Way, Southampton SO14 3ZH, UK; iain.stobbs@soton.ac.uk
[3] Environmental Science Centre, British Geological Survey, Nicker Hill, Keyworth NG12 5GG, UK; plusty@bgs.ac.uk
* Correspondence: berit.lehrmann@noc.ac.uk; Tel.: +44-2380-596263

Received: 15 May 2018; Accepted: 4 July 2018; Published: 18 July 2018

Abstract: Over the last decade there has been an increasing interest in deep-sea mineral resources that may contribute to future raw metal supply. However, before seafloor massive sulfides (SMS) can be considered as a resource, alteration and weathering processes that may affect their metal tenor have to be fully understood. This knowledge cannot be obtained by assessing the surface exposures alone. Seafloor drilling is required to gain information about the third dimension. In 2016, three extinct seafloor massive sulfide mounds, located in the Trans-Atlantic Geotraverse (TAG) hydrothermal area of the Mid-Atlantic Ridge were drilled. A mineralogical and textural comparison of drill core and surface-grab samples revealed that in recent ceased mounds high-temperature copper assemblages typical for black smoker chimneys are still present whereas in longer extinct mounds the mineralogy is pre-dominated by an iron mineral assemblage. Zinc becomes remobilized early in the mound evolution and forms either a layer in the upper part of the mound or has been totally leached from its interior. Precipitation temperatures of sphalerite calculated using the Fe/Zn ratio can help to identify these remobilization processes. While the Fe/Zn ratios of primary sphalerites yield temperatures that are in very good agreement with fluid temperatures measured in white smokers, calculated temperatures for sphalerites affected by remobilization are too high for SMS. Overall drilling of SMS provides valuable information on the internal structure and mineralogy of the shallow sub-surface, however, additional drilling of SMS, at a greater depth, is required to fully understand the processes affecting SMS and their economic potential.

Keywords: extinct seafloor massive sulfides; drilling; TAG hydrothermal area; Mid-Atlantic Ridge

1. Introduction

Since the discovery of the first hydrothermal venting at the Galápagos Rift in 1977 [1], the number of discovered vent sites globally has been steadily increasing with more than 600 sites now known in the oceans [2]. The formation of modern black smoker deposits is related to processes that have occurred on Earth since Archean times [3] and are well understood [4]. However, it remains unknown how seafloor massive sulfides (SMS) are affected by alteration and weathering processes once hydrothermal activity ceases, and what impact this has on their economic potential, that is, whether metal tenors become enriched, depleted, or entirely lost.

Current studies, using bulk geochemical data from 95 sites published in the literature [5,6], suggest a global resource potential for modern SMS deposits along the neovolcanic zones of the seafloor of 600 million tons, with a median grade of 3 wt % Cu, 9 wt % Zn, 2 g/t Au, and 100 g/t Ag [5,6]. However, the geochemical data being used largely originated from easily recoverable, mainly

non-in-situ, surface-grab samples such as high temperature chimneys and their talus material, and are hence not representative of the whole deposits [2,6]. In addition, information regarding thickness and continuity of individual sulfide layers is often inferred from video-surveys and knowledge from volcanic massive sulfides, the ancient analogues to SMS, as few SMS deposits have been drilled to date [7–10].

As a result of the increasing interest in deep-seabed exploration over the last decade, SMS deposits need to be properly assessed to determine whether these deposits can contribute to the growing global demand for natural resources, particularly those metals used in the electronic and green industry. In 2014 the EU-funded "Blue Mining" project was initiated to provide "breakthrough solutions for a sustainable deep-sea mining chain". For the Blue Mining project, the Trans-Atlantic Geotraverse (TAG) hydrothermal field on the Mid-Atlantic Ridge (MAR) was selected as a study area, as it represents one of the best studied hydrothermal systems on earth [11–17]. At 26°08′ N on the MAR (Figure 1), the TAG is one of the largest known hydrothermal systems, with several active and relict hydrothermal zones present in an area of 5 × 5 km, located on the eastern side of the axial valley. Sulfide mounds in this area vary in size, age, and stage of development.

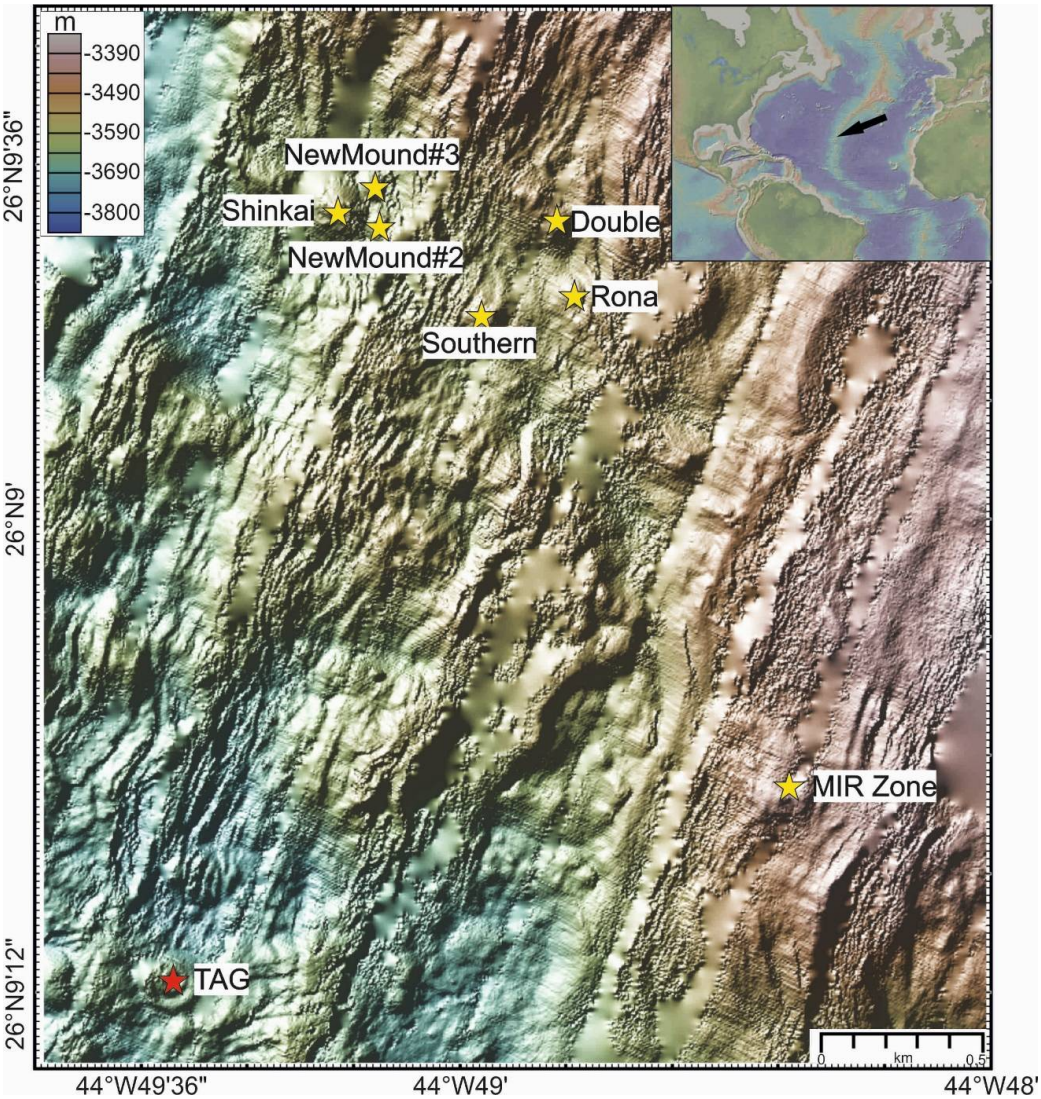

Figure 1. Bathymetric map (data source GeoMapApp: KN142-05 (TAG94), DSL120 2 m grid White) of the Trans-Atlantic Geotraverse (TAG) hydrothermal area and the location of the active and inactive hydrothermal sites studied in the Blue Mining project. The inset shows the location on the Mid-Atlantic.

The active TAG Mound, located in the southwest of the area, comprises two distinct zones. These are the so-called "upper platform" in the northwestern part of the mound and "lower platform", also referred to as Kremlin area in the southeastern part of the TAG mound. Multiple chimneys discharge metal-rich black smoke at a temperature of 365 °C [17] on the upper platform. On the lower platform, there is low temperature diffuse flow, with zinc-rich chimneys and current fluid temperatures of about 50 °C that have decreased from about 270 °C since the 1990s [17]. Mineralization typically encountered here comprises chalcopyrite, pyrite, and anhydrite-rich massive sulfides on the upper platform, and sphalerite-marcasite-pyrite-silica-rich massive sulfides on the lower platform [18]. Sub-surface massive pyrite breccia occurs in the upper part of the mound that gives way at depth to anhydrite-rich pyrite breccia [7]. Deeper in the mound, the anhydrite has been replaced by quartz. The deepest known parts consist of altered wallrock and basalt with the deepest hole recovering altered basalt at 125 m below seafloor (mbsf). At the active TAG Mound, minerals of economic interest only seem to be enriched in the upper five metres [13] whereas at depth a barren massive pyrite body occurs. Similar observations are made for the upper part of volcanic hosted massive sulfide deposits on Cyprus [19]. In addition to the active TAG mound, there are several hydrothermally extinct mounds to the north-northeast: for example, Shinkai Mound, Double Mound, Rona Mound, New Mound #2, New Mound #3 (New M. #2 & #3), Southern Mound, as well as the MIR Zone located two kilometers to east-northeast of the active TAG mound (Figure 1).

Radiometric data indicate that hydrothermal activity started at the active TAG mound 50 ka ago with episodic periods of activity of tens to hundreds of years [20] characterized by accumulation of sulfides and anhydrite, replacement and refining, and hydrothermally inactive periods of 3000 to 5000 years that are characterized by mass wasting, dissolution of anhydrite, and brecciation. Currently, the active TAG Mound is in a high-temperature hydrothermal phase with activity having started 80 years ago [21]. The MIR Zone is the oldest area, with hydrothermal activity first starting 140 ka ago and the last active episode ceasing 0.6 ka ago [20] whereas sulfides from Double and Shinkai Mound yield ages of 50 ka and 2–23 ka, respectively [20]. No radiometric data are available for Rona Mound, Southern Mound, New M. #2 & #3. However, based on the proximity of New M. #2 & #3 to Shinkai Mound and Rona Mound and Southern Mound to Double Mound, and similar slope angles [22], that indicated the degree of anhydrite dissolution at depth [13], similar development stages are assumed for this study.

In 2016, detailed studies of inactive hydrothermal activity and associated extinct seafloor massive sulfides (eSMS) of the TAG area were conducted. A robotic, lander-type seafloor drilling rig (RD 2) from the British Geological Survey was deployed from the British research vessel *RRS James Cook* during cruise JC138. In this paper we compare the nature and mineralogy of surface and sub-surface ore types from a modern, active SMS system at the TAG site provided by ODP (Ocean Drilling Program) drilling [7] with extinct SMS investigated during "Blue Mining" cruise JC138. The aim is to gain information on how hydrothermal alteration and seafloor weathering change the composition of extinct SMS over time and what implications this may have on the economic potential. The results of this surface sampling and drilling campaign add significantly to our understanding of the nature of the shallow sub-seafloor of eSMS and provide detailed information on composition and mineralogy of eSMS that contrasts with the composition of active chimneys.

2. Materials and Methods

During *RRS James Cook* cruise JC138 visual seafloor investigations and 29 surface samples were obtained at Rona Mound, Southern Mound, Shinkai Mound, New M. #2 & #3 using a multipurpose robotic underwater vehicle (HyBIS) from the National Oceanography Centre. In addition, eight holes were drilled on the plateaus of three extinct mounds (Southern Mound, Rona Mound, and MIR Zone) using RD2 (Figure 2). A total of 9.5 m of core was recovered and a maximum penetration of up to 12.5 m below seafloor was achieved. The true core depth was reconstructed from the drill telemetry data recorded.

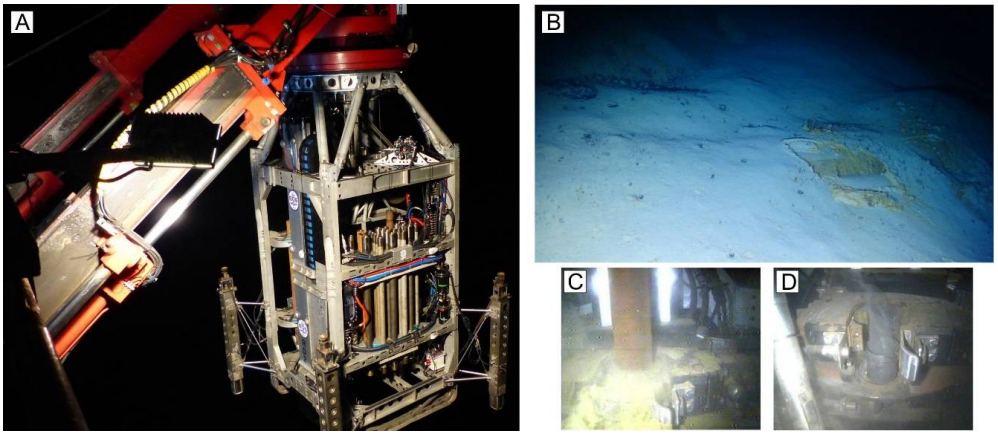

Figure 2. Photographs from the drilling campaign during JC138. (**A**) Deployment of BGS's RD2 using its own launch and recovery system. (**B**) Footprints of the legs of RD2 on pelagic sediment covering Southern Mound. (**C**) Drilling at Rona Mound. (**D**) Sulfide-rich drill cuttings emanating from a borehole at MIR Zone.

After recovery, samples were handled following the protocol established for cruise JC138 [22]. Where possible, sample orientation (i.e., top and bottom) were marked on the sample, and respected during any further steps. The exteriors of all samples were then petrographically described before being cut using a rock saw. Samples were further texturally and mineralogically described and subsamples were subsequently taken for further studies onshore. All samples were dried and individually packed together with oxygen and silica-gel moisture absorbers in evacuated lay-flat polythene tubes and stored at 4 °C in a reefer container to prevent oxidation. Based on surface location, sub-surface depth, textural appearance, and macroscopically identifiable mineralogy, a total of 73 polished thin and thick Sections were prepared and studied under transmitted and reflected light using a MEIJI MX microscope with the attached Infinity 1 camera system. The relative mineralogical compositions were estimated, at a micro-scale, for each sample and an average composition derived for the mounds interior and exterior.

Major element analyses of sulfide minerals were performed on a Cameca-SX100 5-spectrometer microprobe (EMPA, University of Edinburgh) and a Zeiss Sigma HD Field Emission Gun Analytical scanning electron microscope (SEM, Cardiff University). Sulfides were analyzed using 20 kV accelerating voltage, 10 nA beam current (S, Zn), and 100 nA (Fe) and a 1 µm beam diameter. For SEM analyses, the Oxford Instruments 150 mm^2 energy dispersive X-ray spectrometer was used with an acceleration potential of 15 kV. Calibration of EMPA and SEM was performed on natural minerals (pyrite: Fe, S; sphalerite: Zn) on a daily basis. The SEM data are normalized to 100%, automatically, and a direct comparison with EMPA data from the same sample demonstrated that quantitative data from this specific SEM are of comparable quality to that obtained by EMPA. By comparison, using an older generation of SEM (FEI XL30 Field Emission Gun Environmental SEM, Cardiff University), elemental analyses for sphalerite provided only semi-quantitative results and were not used in the geothermometry calculations.

Sphalerite minimum precipitation temperatures were calculated using the equation $Fe/Zn_{sphalerite} = 0.0013\ (T) - 0.2953$ of [23] for each individual sample. This geothermometer is based on the assumption that the uptake of iron into the sphalerite lattice is temperature dependent [24]. According to [23] this geothermometer should only be used for samples from sediment-starved sites. This argument is valid for samples from the TAG area as the MIR Zone as well as the Alvin Zone that hosts the Rona Mound, Southern Mound, Shinkai Mound, and New M. #2 & #3 are classified as a sediment-free tectonic settings [25]. In addition, samples should not have been affected by metamorphic overprint higher than upper greenschist fazies [23], which is also valid for our samples. Furthermore, [23] states that samples should not have been affected by Zn mobilization, which could

be identified by the presence of chalcopyrite and pyrite inclusions in the sphalerite. As no visible inclusions of chalcopyrite and pyrite are present in the samples of this study, the argument of [23] remains valid in the study.

Average and standard deviation were calculated on the fully quantitative sphalerite data set for the two identified sphalerite types for each of the individual mounds.

3. Results

3.1. Seafloor Observations from the Extinct Mounds

The youngest mounds, Shinkai Mound and New M. #2 & #3 are only covered by a thin layer of sediment comprising a mixture of pelagic and weathered iron-rich hydrothermal material that is generally restricted to the flanks of the mounds and small depressions between the mounds. Southern Mound and Rona Mound, that are assumed to be older based on their proximity to Double Mound, are cut by NE–SW-trending, arcuate faults. They are covered by a layer of sediment up to 3 m thick. This comprises a thin layer of pelagic material transitioning into red-brown material of hydrothermal origin at depth (Figure 3A). On the summit of Shinkai Mound, as well as New M. #2 & #3, upright, extinct chimneys are observed, whereas on the flanks chimney relicts and boulder-sized talus material that is mixed with sulfide-rich sediments occurs (Figure 3B). These angular sulfide blocks are generally coated by a thin weathering crust (Figure 3C), comprising iron-oxyhydroxides, jarosite, and copper chloride (atacamite/paratacamite).

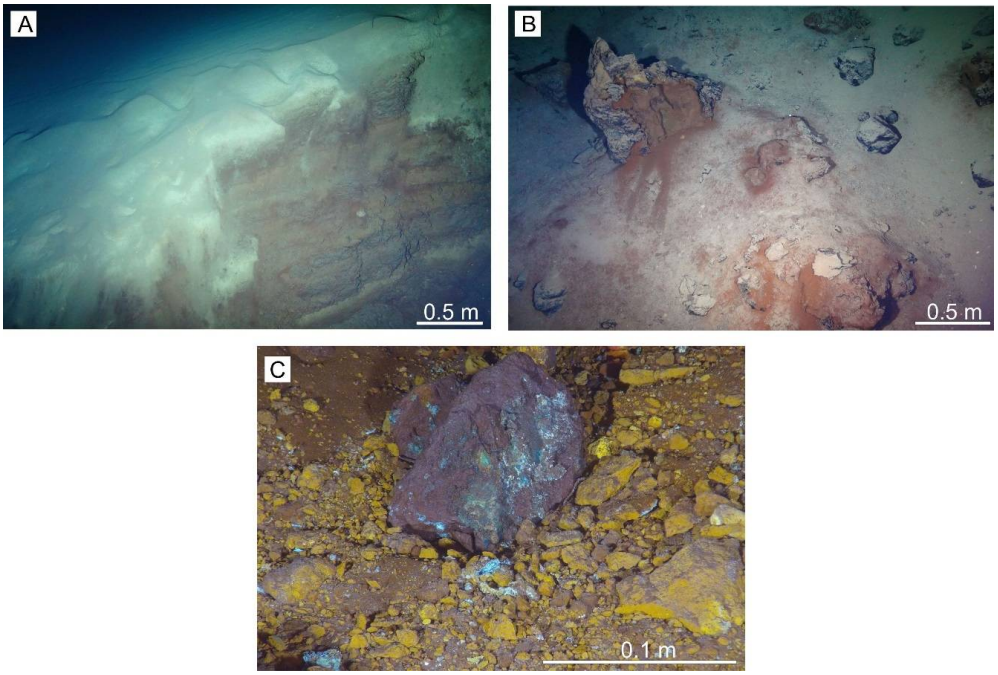

Figure 3. Photographs of seafloor features observed at extinct seafloor massive sulfides (eSMS) sites in the Trans-Atlantic Geotraverse (TAG) hydrothermal area. (**A**) Pelagic sediment underlain by reddish-brown hydrothermal sediment in a fault scarp at Southern Mound, 45HyBIS. (**B**) Upright relict chimney on top of New Mound #2, 55HyBIS. (**C**) Sulfide talus coated by copper-chloride (greenish), jarosite (yellowish-brown) and iron-oxyhydroxide (reddish-brown) at Southern Mound, 41-HyBIS.

3.2. Petrography of Surface Samples

Massive sulfides recovered from the surface of Shinkai Mound and New M. #2 & #3 comprise chimneys and fragments of chimney material whereas samples from Southern Mound and Rona Mound comprise sulfide breccia and massive sulfide blocks (Figure 4). The exterior of almost all

the samples is coated by a thin red-brown iron-oxyhydroxides layer that is associated with greenish copper-chloride and yellowish-brown jarosite. The innermost part of the chimney sample, obtained from New Mound #2 (Figure 4A), comprises an orifice that is lined by idaite (Figure 5A). Extending outwards, coarse-grained tetrahedral chalcopyrite is present that is altered to covellite along grain boundaries adjacent to the idaite. Other chimney material obtained from New Mound #3 comprises coarse-grained chalcopyrite that hosts micro-meter sized Fe-rich sphalerite inclusions (average Fe: 10.4 wt %, n = 9). Exsolution lamella of isocubanite (Figure 5B) can also be observed. Pyrrhotite, a common phase in high-temperature chimneys, is absent in the sample from the Shinkai Mound and New M. #2 & #3, however, tabular to lath shaped pseudomorphs now composed of pyrite are present (Figure 5C).

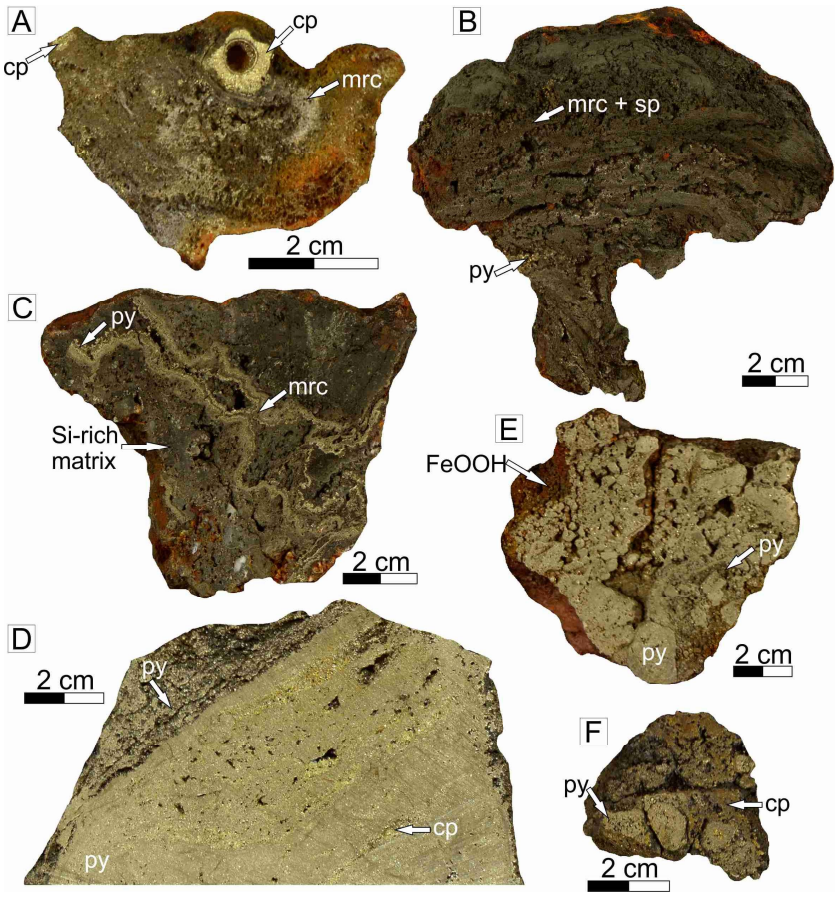

Figure 4. Representative sulfide samples obtained by HyBIS from extinct sulfide mound from the TAG area. (**A**) Chimney with a chalcopyrite-rich orifice surrounded by Cu-Fe-rich sulfides, New M. #2, 55-1. (**B**) Chimney wall fragment comprising marcasite that is intimately intergrown with sphalerite and pyrite, and is coated by amorphous silica (not visible on hand specimen scale), New M. #2, 55-3. (**C**) Chimney talus comprising banded marcasite and pyrite hosted in a silica-rich matrix, Shinkai M., 55-8. (**D**) Massive sulfide talus comprising pyrite with intercalated layers of chalcopyrite, Southern M., 21-3. (**E**) Sulfide breccia comprising angular clasts of pyrite hosted in a pyrite matrix, Southern M., 45-6. (**F**) Sulfide breccia comprising of sub-angular pyrite clasts that are hosted in a chalcopyrite rich matrix, Rona M., 45-7. Mineral abbreviations: cp: chalcopyrite, py: pyrite, mrc: marcasite, sp: sphalerite, Si: amorphous silica/quartz.

Sulfide-rich material, characteristic of the outer wall of a classic black smoker chimney was obtained from New Mound #2 and Shinkai Mound (Figure 4B,C). These samples comprise Fe-poor sphalerite (average 4.17 wt %, n = 6) that is associated with colloform marcasite (Figure 5D) and aggregates of cubic pyrite that are overgrown by colloform marcasite (Figure 5E). In both samples,

the sulfides are coated by a micrometer thick layer of amorphous silica. Anhydrite, typical for high-temperature chimneys and chalcopyrite disease in sphalerite, is absent at all three mounds.

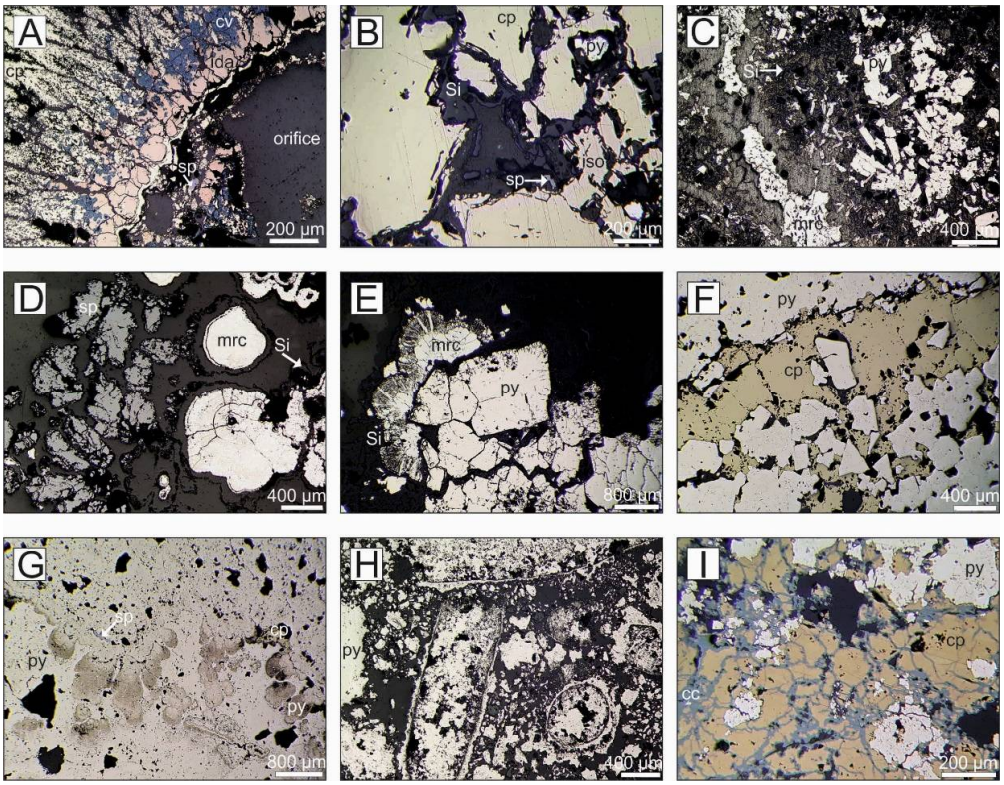

Figure 5. Reflected photomicrographs of representative mineral assemblages and textures from surface samples obtained by HyBIS during cruise JC138. (**A**) Cross-Section of chimney comprising of tetrahedral shaped coarse-grained chalcopyrite, subhedral idaite altered to covellite along grain boundaries, New M. #2, 55-1. (**B**) Coarse-grained chalcopyrite with exsolution lamella of isocubanite and coated by a thin layer of amorphous silica, New M. #3, 055-6. (**C**) Pyrite pseudomorphs after tabular pyrrhotite associated with marcasite, New M. #3, 055-6. (**D**) Radial aggregates to colloform marcasite associated with dendritic sphalerite and coated with thin layer of amorphous silica, New M. #2, 55-3. (**E**) Cubic to subhedral aggregates of pyrite overgrown by colloform marcasite and hosted in amorphous silica, Shinkai M., 55-8. (**F**) Massive recrystallized pyrite with intercalated layer of chalcopyrite, Southern M., 21-3. (**G**) Colloidal aggregates of pyrite overgrown by massive pyrite that host inclusions of sphalerite and chalcopyrite, Southern M., 41-4. (**H**) Fine-grained pyrite with fossil remnants of tube worms, Southern M., 41-6. (**I**) Pyrite clasts surrounded by chalcopyrite that is altered to chalcocite along micro-fractures, Rona M., 45-7. Mineral abbreviations: cp: chalcopyrite, iso: isocubanite/cubanite, ida: idaite, cc: chalcocite, cv: covellite, py: pyrite, mrc: marcasite, sp: sphalerite, Si: amorphous silica/quartz.

Surface samples from Southern and Rona Mound contrast with Shinkai Mound and New M. #2 & #3 as massive sulfides and sulfide breccia (Figure 4D–F) dominate. In the massive sulfide blocks pyrite forms massive recrystallized aggregates that are either intercalated with chalcopyrite layers (Figure 5F) or overgrow earlier porous colloform pyrite (Figure 5G). Within the recrystallized pyrite, inclusions of Fe-rich sphalerite (average Fe: 12.74 wt %, $n = 7$) and chalcopyrite can be observed. The sulfide breccia comprises angular to sub-angular clasts formed of aggregates of recrystallized pyrite that are hosted in a pyrite matrix. Rare fossil remnants of tube worms that are replaced by pyrite can be identified in the breccia (Figure 5H). At Rona Mound the breccia comprises angular pyrite clasts, hosted in massive chalcopyrite that has been altered along micro-fractures to chalcocite (Figure 5I). Rare rosettes of barite occur in vugs.

3.3. Petrography of Sub-Surface Samples

Drill core recovery from three eSMS mounds varies (Figure 6), ranging from 1.4% at site 068RD to 72.5% at site 031RD. The uppermost lithological layer consists of pelagic sediment where it was observed during HyBIS dives (Figure 3A) and accidentally sampled by the legs of RD2 (Figure 2B) indicating a thickness of approximately 20 cm. The pelagic sediment is underlain by 0.7–3.5 m of orange to red-brown hydrothermal sediment. Beneath the sediment a layer of jasper, up to three meters thick occurs. At Southern Mound and Rona Mound, this is intercalated with a layer of jasper–silica breccia (i.e., angular jasper clasts in a silica/quartz matrix) that is up to 0.5 m thick. However, this appears to be absent in the MIR Zone. In addition, at the MIR Zone a 0.1 cm thick layer comprising iron-oxyhydroxides can be observed between the hydrothermal sediments and jasper.

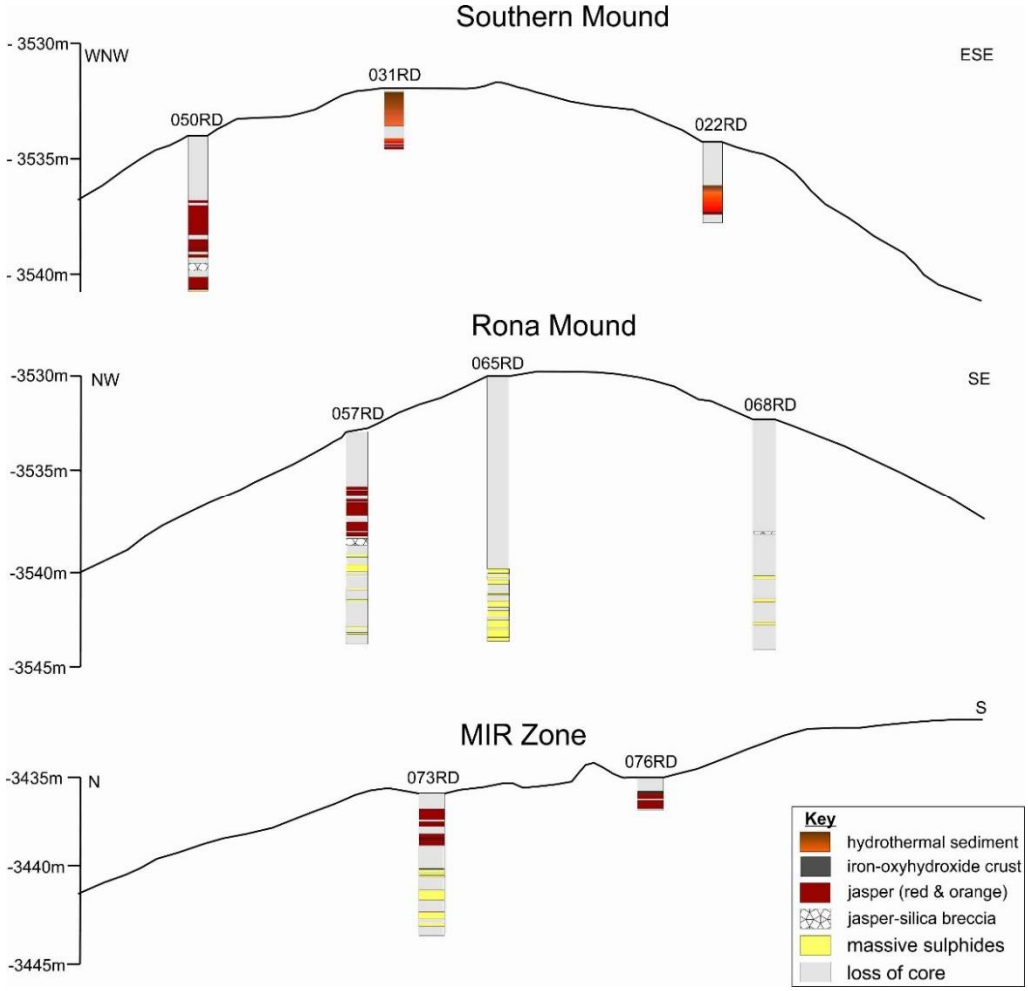

Figure 6. Schematic cross-Section through Southern Mound, Rona Mound, and MIR Zone, drilled during Blue Mining cruise JC138, using RD2 from the BGS.

The jasper is underlain by massive sulfides at 3.6 mbsf at MIR Zone, 6 mbsf at Rona Mound and 6.6 mbsf at Southern Mound. At Southern Mound, only a pebble of massive sulfide was recovered (Figure 7A) that comprises massive pyrite with intercalated layers of chalcopyrite. Sulfides from Rona Mound are more diverse. The upper three meters of intersected sulfides (6–9 mbsf) are vuggy (up to 25% porosity) and comprise of Fe-poor sphalerite (average Fe: 2.88 wt %, n = 33), marcasite, and pyrite. These minerals form rhythmic colloform zones and overgrow framboidal pyrite (Figure 8B,C). A second generation of pyrite exhibits massive recrystallized textures and surrounds the earlier marcasite–sphalerite assemblage. Barite forms rosettes that occur in interstices of the sulfides. Another

accessory phase in the upper part of the sulfides of Rona Mound is amorphous silica that coats the sulfides with a micro-meter thick layer. Beneath the Zn-rich sulfide assemblage massive pyrite that is associated with chalcopyrite occurs (Figure 7C,D). This mineral assemblage is also present in sulfides in the MIR Zone (Figure 7E). At Rona Mound, porous colloform pyrite is overprinted by massive pyrite that itself is overgrown by coarse-grained aggregates of pyrite (Figure 8E,G). Chalcopyrite either overprints the pyrite, or is found as inclusions (Figure 8D) in association with Fe-poor sphalerite (average Fe: 4.41 wt %, $n = 7$).

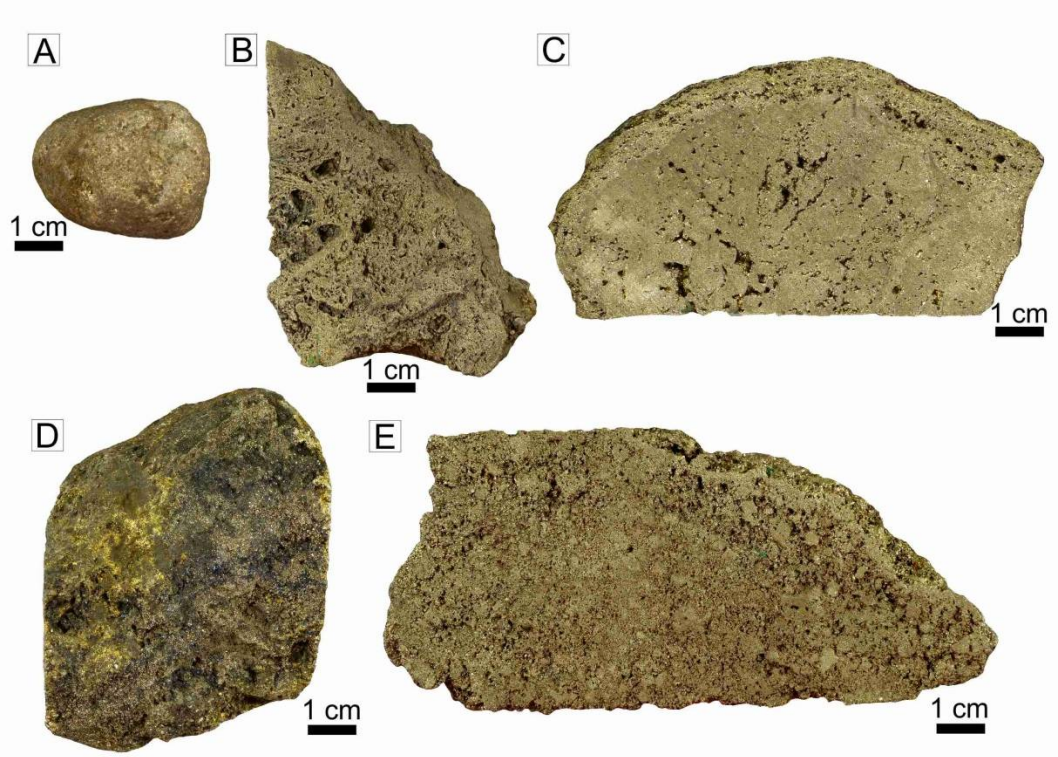

Figure 7. Representative drill core samples from the three eSMS mounds drilled during Blue Mining cruise JC138. (**A**) Sulfide pebble comprising pyrite and chalcopyrite (Southern M., 50-14, 6.63–6.73 mbsf). (**B**) Vuggy massive sulfide comprising marcasite and sphalerite (Rona M., 57-19, 7.09–7.26 mbsf). (**C**) Massive sulfide predominately consisting of pyrite with thin intercalated chalcopyrite layer (Rona M., 65-23, 12.32–12.41 mbsf). (**D**) Massive pyrite with chalcopyrite on a fractured surface (Rona M., 65-2, 9.36–9.59 mbsf). (**F**) Sulfide breccia comprising pyrite hosted in a matrix of chalcopyrite (MIR Zone, 073-29, 6.96–7.12 mbsf).

Even at 12 mbsf, rosettes of barite can be observed at sulfide grain interstices (Figure 8F) where the barite seems to surround earlier chalcopyrite that has been altered to covellite along its grain boundaries. At the MIR Zone, pyrite also exhibits a porous colloform texture (Figure 8I) that is overgrown by massive recrystallized pyrite. Chalcopyrite occurs in interstices or surrounds earlier cubes of coarse-grained pyrite (Figure 8H). Very rare micro-sized inclusions of Fe-rich sphalerite (average 17.09 wt %, $n = 2$) are present in the pyrite.

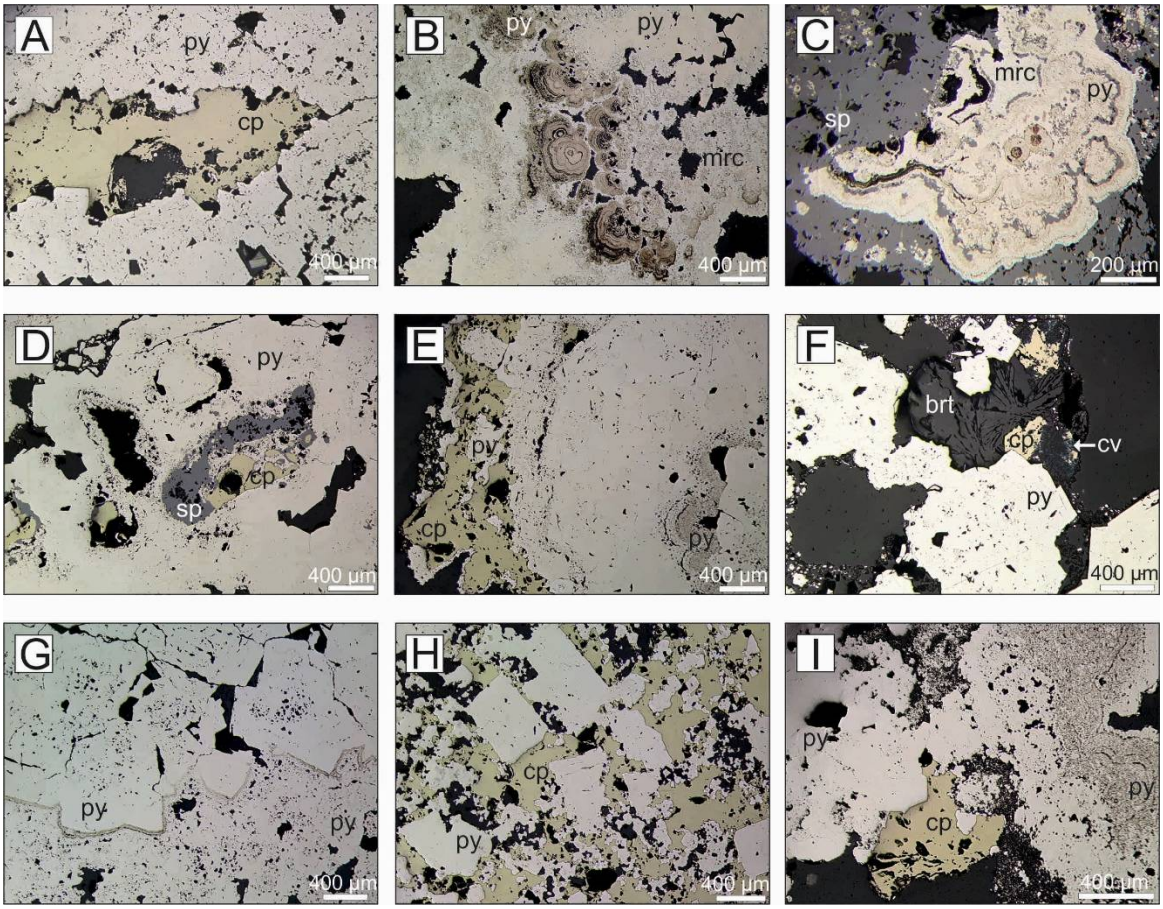

Figure 8. Reflected light photomicrographs of representative mineral assemblages and textures from drill core samples obtained during JC138. (**A**) Massive recrystallized pyrite with intercalated layers of chalcopyrite (Southern M., 50-14, 6.63–6.73 mbsf). (**B**) Colloidal pyrite overgrown by marcasite and later pyrite (Rona M., 57-12, 6.37–6.48 mbsf). (**C**) Framboidal pyrite overgrown by rhythmic bands of colloform marcasite and sphalerite and surrounded by sphalerite (Rona M., 57-19, 7.09–7.26 mbsf). (**D**) Massive recrystallized pyrite overgrowing sphalerite and chalcopyrite (Rona M., 65-11, 11.20–11.29 mbsf). (**E**) Porous colloform pyrite overgrown by pyrite and later chalcopyrite (Rona M., 57-27, 10.37–10.55 mbsf). (**F**) Rosette of barite filling pore space and overgrowing chalcopyrite that is partly altered to covellite along grain boundaries (Rona M., 65-20, 12.08–12.14 mbsf). (**G**) Porous pyrite that is overgrown by massive recrystallized pyrite (Rona M., 65-23, 12.32–12.41 mbsf). (**H**) Cubic pyrite surrounded by chalcopyrite (MIR Zone, 73-18, 4.32–4.38 mbsf). (**I**) Porous colloform pyrite that is overgrown by recrystallized pyrite with chalcopyrite occurring in the pore space (MIR Zone, 73-22, 5.28–5.47 mbsf). Mineral abbreviations: cp: chalcopyrite, cv: covellite, py: pyrite, mrc: marcasite, sp: sphalerite, brt: barite.

3.4. Iron-Content of Sphalerite and Formation Temperatures

Sphalerite from the extinct mounds in the TAG hydrothermal area can be classified into two types. Type-1 comprises one of the principal phases and is predominately associated with marcasite in sub-surface samples from Rona Mound and in chimney material from Shinkai Mound and New M. #2 & #3. Analysis of this sphalerite reveals that it has a low iron-content (Table 1), ranging from 0.82–8.96 wt %. Type-2 comprises inclusions of sphalerite hosted in pyrite and chalcopyrite. These sphalerites are either iron-poor (Rona Mound) or iron-rich at MIR Zone, Shinkai Mound, and New M. #2 & #3. Based on the temperature-dependent uptake of iron into the sphalerite lattice [24], it is possible to calculate formation temperatures of the sphalerite [23].

Table 1. Chemical composition of sphalerite from the TAG area obtained during Blue Mining cruise JC138.

		Element (wt %)			
		Fe	**Zn**	**S**	**Temperature (°C) ***
		Average ± STDEV	**Average ± STDEV**	**Average ± STDEV**	**Average ± STDEV**
Location (Analyes)	Type	**Min.–Max.**	**Min.–Max.**	**Min.–Max.**	**Min.–Max.**
Shinkai/New Mounds (6) surface samples	main phase	4.17 ± 1.91 **0.82–6.77**	63.00 ± 1.94 **60.86–65.66**	32.83 ± 0.69 **31.75–33.52**	279 ± 25 **237–313**
Shinkai/New mounds (9) surface samples	inclusion	10.40 ± 5.62 **4.28–19.84**	57.57 ± 6.30 **46.71–63.84**	32.03 ± 1.16 **30.70–34.20**	377 ± 100 **279–554**
Southern/Rona (7) surface samples	inclusion	12.74 ± 4.18 **7.21–17.99**	53.56 ± 4.17 **48.39–59.64**	33.70 ± 0.83 **32.04–34.59**	416 ± 74 **320–513**
Rona (33) drill core	main phase	2.88 ± 2.39 **0.41–8.96**	64.00 ± 2.61 **57.00–66.63**	33.08 ± 0.43 **32.07–34.01**	263 ± 32 **232–348**
Rona (7) drill core	inclusion	4.41 ± 2.72 **2.08–10.71**	62.61 ± 2.91 **56.18–65.35**	32.97 ± 0.57 **32.07–33.84**	283 ± 39 **252–374**
MIR Zone (2) core	inclusion	17.09 ±1.26 **15.83–18.34**	48.93 ± 1.36 **47.57–50.29**	33.99 ± 0.11 **33.88–34.09**	497 ± 27 **469–524**

All data were obtained using the SEM with the exception of Rona drill core where an electron microprobe was used.
* Temperatures calculated using $Fe/Zn_{sphalerite} = 0.0013\ (T) - 0.2953$ [23].

Type-1 sphalerite from Shinkai Mound and New M. #2 & #3 and Rona Mound, and the sphalerite inclusions in drill core samples from Rona Mound, yield temperatures that range between 263 °C to 283 °C. Sphalerite inclusions found in samples from the MIR Zone, Shinkai Mound and New M. #2 & #3 and surface samples from Southern and Rona Mound yield higher temperatures ranging from 377 °C to 497 °C.

4. Discussion

4.1. Sulfide Mineralogy and Textures

The polymetallic, coarse-grained mineral assemblages (i.e., chalcopyrite, isocubanite, idaite, pyrite, marcasite) observed within surface samples from Shinkai Mound and New M. #2 & #3 are similar to those observed in the black smoker complex at the active TAG Mound (Figure 9). Although pyrrhotite and anhydrite, which are representative of the early stage of black smoker formation [4] are absent, tabular pseudomorphs now comprising pyrite indicate that pyrrhotite may have been present at an earlier stage of development, but has been oxidized and replaced by a more stable phase. The chalcopyrite-isocubanite assemblage, formed through the breakdown of an intermediate solid solution, suggests that the chimney-type samples were formed at high temperatures, ranging between 280 °C to 350 °C [4,26]. This is validated by the mineral assemblage comprising chalcopyrite and idaite observed in another chimney sample and data arising from previous work that suggests this assemblage forms at temperatures of 300–350 °C [27].

Further chimney material, recovered from the Shinkai Mound and New M. #2 & #3, and drill core from the upper sulfide layer at Rona Mound comprises dendritic sphalerite that is associated with colloform marcasite and overgrow framboids of earlier pyrite. The presence of framboidal pyrite suggests that the iron-disulfide was precipitated from supersaturated hydrothermal fluids, at temperatures of <150 °C [29] or 200 °C [30], which are typical of the initial phase of black smoker growth [4]. Marcasite, that is overgrowing the earlier framboidal pyrite, forms at temperatures of <240 °C [31]. It is associated with sphalerite forming a typical white smoker mineral assemblage [4] and forms between 250–175 °C [26].

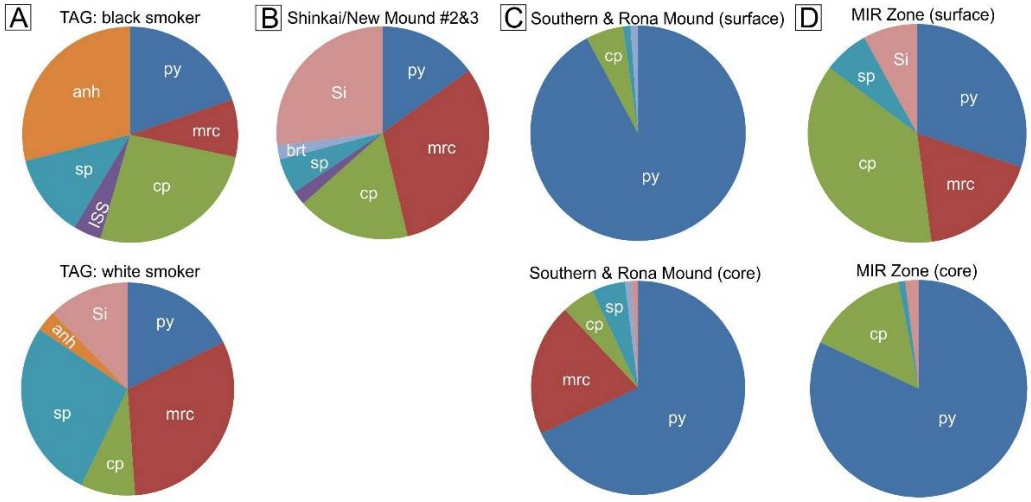

Figure 9. The relative abundance of major minerals observed in surface and sub-surface samples from the TAG area. (**A**) Typical minerals occurring in black and white smoker samples recovered from the active TAG mound, data from [18]. (**B**) Typical mineral assemblage in surface grab-samples from Shinkai Mound and New M. #2 & #3 obtained during Blue Mining cruise. (**C**) Composition of surface and subsurface samples from Southern Mound and Rona Mound obtained during Blue Mining cruise. (**D**) Typical mineral assemblage in surface (data from [12,28]) and sub-surface samples (data from Blue Mining cruise) from the MIR Zone. Mineral abbreviations: cp: chalcopyrite, ISS: isocubanite/cubanite, py: pyrite, mrc: marcasite, sp: sphalerite/wurtzite, anh: anhydrite, brt: barite, Si: amorphous silica/quartz.

Coarse-grained, recrystallized, occasionally euhedral pyrite encountered in the MIR Zone and the deeper parts of Rona Mound suggest that the primary mineral assemblage reacted with hotter, more reduced fluid that could precipitate chalcopyrite [32]. The presence of an amorphous silica coating indicates that the sulfide assemblages are likely to have formed from supersaturated fluids at temperatures <200 °C [33]. Nevertheless this coating helps to protect the sulfides from extensive oxidation by ingressing ambient seawater. However, the presence of barite indicates that seawater was able to penetrate into the deposits, to depths of at least 12 mbsf. Furthermore, the formation of covellite and chalcocite along micro-fractures and grain boundaries indicates the presence of an oxidizing and more acidic, low temperature fluid (<150 °C) in the system [34,35]. In addition, the absence of anhydrite, that is quite abundant at the active TAG mound, suggests that fluid temperatures dropped below <150 °C, at which anhydrite becomes unstable [36].

The sulfide breccia formed during various stages of the mound growth. Anhydrite associated with chimneys dissolved when temperatures dropped below 150 °C resulting in collapsing of the sulfide edifices on the surface but also within the mounds wherever seawater was able to penetrate into its interior, for example, along faults. This process causes extensive in-situ brecciation [37], mass wasting, and ultimately the formation of sulfide sands [13]. For the samples in this study, mass wasting appears to be a minor process as the presence of angular clasts indicates a transport of short distances. Low temperature diffuse flow caused cementation of the sulfides, as observed in samples from Southern Mound and Rona Mound (Figure 4E,F). Within the mounds, sulfides zone refining is present that was caused by late-stage, upwelling, Cu-rich, high-temperature fluids [38]. This acidic fluid was capable of remobilizing zinc along the steep thermal gradient, that is, moving it to cooler, outer parts of the mounds [37,39] and simultaneously precipitating Fe sulfides and chalcopyrite [38].

4.2. Sphalerite Precipitation Temperatures

The validity for the geothermometer for our samples was verified prior to application (see material and methods). Type-1 sphalerite, that is only present in Shinkai Mound, New M. #2 & #3, Southern Mound and Rona Mound, yield average temperatures of 279 ± 25 °C and 263 ± 32 °C, respectively. The temperatures are slightly higher than the temperatures of 250–175 °C suggested in the literature [26]. However, measurements in the 1990s of white smoker vent fluids at the active TAG Mound recorded temperatures of 270 °C [17] and are in very good agreement with the calculated temperatures from this study. As type-1 sphalerites exhibit dendritic and colloform textures that indicate a direct precipitation from the hydrothermal fluid [40] it can be proposed that these sphalerites are the primary generation and not formed through later remobilization processes. Type-2 sphalerites, present in inclusions, are more complex. At Shinkai Mound, New M. #2 & #3, Southern Mound, and Rona Mound the average temperatures are 377 ± 100 °C and 416 ± 74 °C, respectively. The large standard deviation indicates that inclusions are heterogeneous with regards to their iron/zinc ratio. As the host mineral of these inclusions are coarse-grained, mainly recrystallized pyrite and chalcopyrite, it is proposed that remobilizing and recrystallizing processes affected the sphalerite chemistry yielding temperatures that are too high. Sphalerite inclusions of the MIR Zone appear also to have been altered by remobilizing and recrystallizing processes with their average temperature of 497 ± 27 °C too high for black smoker systems. Inclusions of sphalerite in drill core from Rona Mound are hosted in pyrite and chalcopyrite from the copper-rich zone and yield an average formation temperature of 283 ± 39 °C. This result is within the range of standard deviation from the type-1 sphalerite from this site and it is proposed that these inclusions have not experienced any loss of zinc.

4.3. Evolution of Extinct Seafloor Massive Sulfide Deposits

The active TAG Mound represents the earliest formation stage of an SMS deposit with black and white smoker fluids being discharged its surface chimneys (Figure 10A). Massive sulfides and breccia recovered from the upper 15 m below the surface during ODP drilling in the 1990's [7] reflect metal remobilization and re-precipitation caused by multiple hydrothermal events of different temperature [14]. These caused zone refining and metal enrichment in the upper 5 m of the mound [13]. In addition, dissolution of anhydrite created void space and resulted in collapse of the mound and brecciation. Currently, the TAG Mound is active and high-temperature (>350 °C), copper-rich metal assemblages still form.

Shinkai Mound and New M. #2 & #3 (Figure 10B) represent the first stage after high-temperature hydrothermal activity has ceased. Although these mounds were not drilled during the Blue Mining cruise, petrological and mineralogical observations are important as the Shinkai Mound and New M. #2 & #3 represents the intermediate step between an active system and a long deceased system. Copper-rich, high-temperature minerals and assemblages, typical of white smokers, are still present. Talus samples recovered from the mounds only comprise chimney fragments, rather than massive sulfide blocks or breccia, suggesting that anhydrite is still present in the interior of the deposit as otherwise the upper-mound surface would have flattened [13]. Since these mounds were not drilled during this study, it remains unknown whether metal zonation occurs in the sub-surface.

The model for Southern Mound and Rona Mound (Figure 10C) implies that the upper part of the mounds has undergone zone refining, with a zinc-rich sulfide layer being underlain by copper-rich sulfides, like at the active TAG mound [13]. Since this metal zonation is also observed in other SMS systems that have been drilled, such as Bent Hill and Palinuro [8,10], it seems to be a common process in mound evolution. The mound has started to collapse and the surface flattens because of anhydrite dissolution and in-situ brecciation in the mound interior.

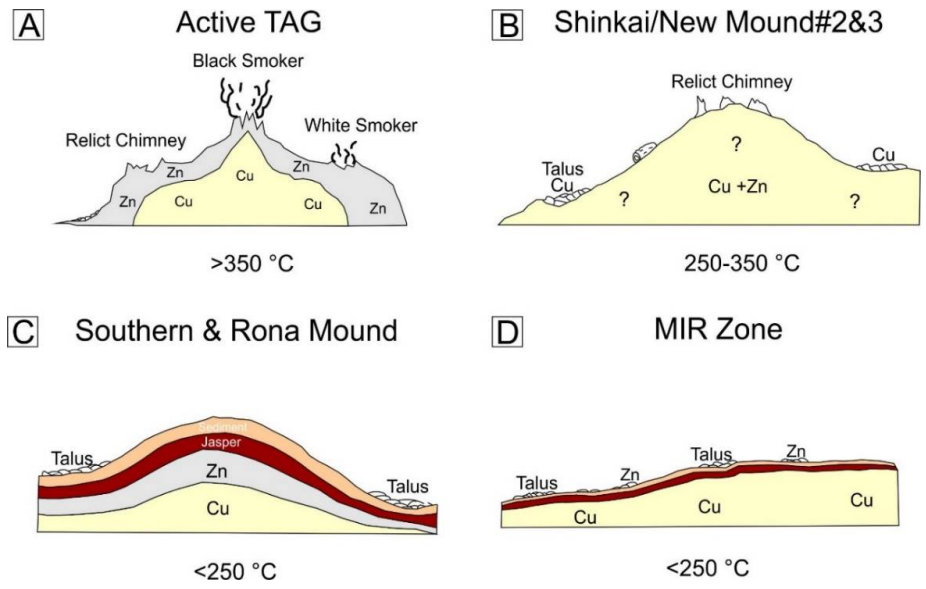

Figure 10. Schematic cross sections of the active TAG Mound and three extinct sites investigated during Blue Mining cruise. (**A**) Active TAG mound with black and white smoker edifices on the surface and metal-rich subsurface zones, modified from [18]. (**B**) Surface and sub-surface model for Shinkai Mound and New M. #2 & #3, with extinct chimneys and talus on the surface and inferred copper- and zinc-rich massive sulfides at depth. (**C**) Sub-surface structure of Southern Mound and Rona Mound, showing zone refining of metals concealed under a sediment-jasper cap. (**D**) Sub-surface model of the MIR Zone, with copper-rich massive sulfides under a thin cap of sediments and jasper. The stated temperatures reflect the state of the system, i.e., >350 °C active black smoker system with copper-rich mineral assemblages, 250–350 °C stand for an inactive system that has not undergone intense alteration yet and <250 °C intermediate to long ceased system with intense metal remobilization and zone refining. Cross sections represent the upper 15 m of the different sites and are not to scale.

The MIR Zone, that represents the oldest identified mound in the TAG area [20], has also undergone interior zone refining (Figure 10D), with the presence of sulfide breccia and a flattened mound shape suggesting anhydrite dissolution has occurred at depth. No-zinc rich layer was encountered in the shallow sub-surface during the drilling campaign, but surface material is enriched in zinc [12,28]. This suggests that that zinc was removed from the shallow sub-surface part of the deposit by a late-stage copper-rich fluid as observed in the other mounds. The presence of such a fluid would explain the presence of chalcopyrite cementing coarse-grained recrystallized pyrite.

5. Conclusions

The results of this surface sampling and shallow sub-surface drilling campaign demonstrate that the composition of eSMS contrasts with the composition of active chimneys. Once hydrothermal activity ceases zone refining processes result in zinc being remobilized or removed from the mounds. Sphalerite precipitation temperatures can help to distinguish primary from remobilized sphalerite as the Fe/Zn ratio become affected by remobilization leading to unrealistically temperatures that are too high for black smoker systems. Copper appears to be preferentially retained within the upper parts of the structure. This suggests that any mineralization of economic interest is restricted to shallow part of eSMS. However, drilling of additional eSMS, and to a greater depth, is required to fully understand the processes controlling the alteration of eSMS deposits as a whole.

Author Contributions: B.J.M., P.A.J.L., I.J.S., and B.L. conceived and designed the shipboard experiments. B.L. performed the onshore experiments and analyses and wrote the manuscript. B.J.M. and P.A.J.L. revised the manuscript.

Funding: This study was supported by a grant from the European Union Seventh Framework Program (EU-FP7) "Blue Mining: breakthrough solutions for the sustainable deep-sea mining value chain" under grant No. 604500. This grant also supported the cruise on RRS James Cook (JC138) in 2016.

Acknowledgments: We acknowledge support from NERC (ship-time), University of Southampton (thin section preparation), Duncan Muir from Cardiff University (SEM-time), Chris Hayward from University of Edinburgh (EMPA-time). Special thanks to Sven Petersen from GEOMAR for his valuable input during Blue Mining cruise JC138. Paul Lusty publishes with the permission of the Executive Director, British Geological Survey (UKRI). We gratefully acknowledge comments provided by two anonymous reviewers.

Conflicts of Interest: The authors declare no conflict of interest. The founding sponsors had no role in the design of the study; in the collection, analyses, or interpretation of data; in the writing of the manuscript, and in the decision to publish the results.

References

1. Corliss, J.B.; Dymond, J.; Gordon, L.I.; Edmond, J.M.; Herzen von, R.P.; Ballard, R.D.; Green, K.; Williams, D.; Bainbridge, A.; Crane, K.; et al. Submarine thermal springs on the Galápagos Rift. *Science* **1979**, *203*, 1073–1083. [CrossRef] [PubMed]
2. Hannington, M.; Jamieson, J.; Monecke, T.; Petersen, S. Modern sea-floor massive sulphides and base metal resources: Toward an estimate of global sea-floor massive sulphide potential. In *The Challenge of Finding New Mineral Resources: Global Metallogeny, Innovative Exploration, and New Discoveries. Vol. 2: Zinc-Lead, Nickel-Copper-PGE, and Uranium*; Goldfarb, R.J., Marsh, E.E., Monecke, T., Eds.; Society of Economic Geologists: Littleton, CO, USA, 2010; Volume 15, pp. 317–338. ISBN 978-1-629496-34-4.
3. Galley, A.G.; Hannington, M.D.; Jonasson, I.R. Volcanogenic massive sulphide deposits. In *Mineral Deposits of Canada: A Synthesis of Major Deposit-Types, District Metallogeny, the Evolution of Geological Provinces, and Exploration Methods*; Goodfellow, W.D., Ed.; Geological Association of Canada: St John's, NL, Canada, 2007; pp. 141–161. ISBN 978-1-897095-24-9.
4. Halbach, P.E.; Fouquet, Y.; Herzig, P. Mineralization and compositional patterns in deep-sea hydrothermal systems. In *Energy and Mass Transfer in Marine Hydrothermal Systems*; Halbach, P.E., Tunnicliffe, V., Hein, J.R., Eds.; Dahlem University Press: Berlin, Germany, 2003; pp. 85–122. ISBN 978-3934504127.
5. Hannington, M.; Jamieson, J.; Monecke, T.; Petersen, S.; Beaulieu, S. The abundance of seafloor massive sulphide deposits. *Geology* **2011**, *39*, 1155–1158. [CrossRef]
6. Monecke, T.; Petersen, S.; Hannington, M.D.; Grant, H.; Samson, I.M. The minor element endowment of modern seafloor massive sulphides and comparison with deposits hosted in ancient volcanic successions. In *Rare Earth and Critical Elements in Ore Deposits*; Verplanck, P.L., Hitzman, M.W., Eds.; Society of Economic Geologists (SEG): Knoxville, TN, USA, 2016; Volume 18, pp. 245–306. ISBN 978-1-62949-218-6.
7. Humphris, S.E.; Herzig, P.M.; Miller, D.J. (Eds.) *Proceedings of the Ocean. Drilling Program.-Initial Report*; Texas A&M University: College Station, TX, USA; Volume 158. [CrossRef]
8. Zierenberg, R.A.; Fouquet, Y.; Miller, D.J.; Normark, W.R. (Eds.) *Proceedings of the Ocean. Drilling Program.-Scientific Results*; Texas A&M University: College Station, TX, USA; Volume 169. [CrossRef]
9. Petersen, S.; Kuhn, K.; Kuhn, T.; Augustin, N.; Hekinian, R.; Franz, L.; Borowski, C. The geological setting of the ultramafic-hosted Logatchev hydrothermal field (14°45′N, Mid-Atlantic Ridge) and its influence on massive sulfide formation. *Lithos* **2009**, *112*, 40–56. [CrossRef]
10. Petersen, S.; Monecke, T.; Westhues, A.; Hannington, M.D.; Gemmell, J.B.; Sharpe, R.; Peters, M.; Strauss, H.; Lackschewitz, K.; Augustin, N.; et al. Drilling Shallow-Water Massive Sulfides at the Palinuro Volcanic Complex, Aeolian Island Arc, Italy. *Econ. Geol.* **2014**, *109*, 2129–2157. [CrossRef]
11. Rona, P.A.; Klinkhammer, G.; Nelsen, T.A.; Trefry, J.H.; Elderfield, H. Black smokers, massive sulfides, and vent biota at the Mid-Atlantic Ridge. *Nature* **1986**, *321*, 33–37. [CrossRef]
12. Rona, P.A.; Bogdanov, Y.A.; Gurvich, E.G.; Rimski-Korsakov, A.; Sagalevitch, A.M.; Hannington, M.D.; Thompson, G. Relict hydrothermal zones in the TAG hydrothermal field, Mid-Atlantic Ridge 26°N, 45°W. *J. Geophys. Res.* **1993**, *98*, 9715–9730. [CrossRef]
13. Hannington, M.D.; Galley, A.D.; Herzig, P.M.; Petersen, S. Comparison of the TAG mound and stockwork complex with Cyprus-type massive sulfide deposits. In Proceedings of the Ocean Drilling Program-Scientific Results, Charleston, SC, USA, 8 January 1997; Herzig, P.M., Humphris, S.E., Miller, D.J., Zierenberg, R.A., Eds.; Texas A&M University: College Station, TX, USA, 2001; Volume 158, pp. 389–415. [CrossRef]

14. Petersen, S.; Herzig, P.M.; Hannington, M.D. Third dimension of a presently forming VMS deposit: TAG hydrothermal field, Mid-Atlantic Ridge, 26° N. *Miner. Depos.* **2000**, *35*, 233–259. [CrossRef]
15. Tivey, M.A.; Schouten, K.; Kleinrock, M.C. A near-bottom magnetic survey of the Mid-Atlantic Ridge axis at 26°N: Implications for the tectonic evolution of the TAG segment. *J. Geophys. Res.* **2003**, *108*, 2277–2789. [CrossRef]
16. DeMartin, B.; Reves-Sohn, R.; Canales, J.P.; Humphris, S.E. Kinematics and geometry of detachment faulting beneath the TAG hydrothermal field, Mid-Atlantic Ridge. *Geology* **2007**, *35*, 711–714. [CrossRef]
17. Humphris, S.E.; Tivey, M.K.; Tivey, M.A. The Trans-Atlantic Geotraverse hydrothermal field: A hydrothermal system on an active detachment fault. *Deep Sea Res. Part II* **2015**, *121*, 8–16. [CrossRef]
18. Hannington, M.; Herzig, P.; Scott, S.; Thompson, G.; Rona, P. Comparative mineralogy and geochemistry of gold-bearing sulfide deposits on the mid-ocean ridges. *Mar. Geol.* **1991**, *101*, 217–248. [CrossRef]
19. Constantinou, G.; Govett, G.J.S. Geology, geochemistry and genesis of Cyprus sulfide deposits. *Econ. Geol.* **1973**, *68*, 843–858. [CrossRef]
20. Lalou, C.; Reyss, J.L.; Brichet, E.; Rona, P.A.; Thompson, G. Hydrothermal activity on a 10^5-year scale at a slow-spreading ridge, TAG hydrothermal field, Mid-Atlantic Ridge 26°N. *J. Geophys. Res.* **1995**, *100*, 17855–17862. [CrossRef]
21. Lalou, C.; Reyss, J.L.; Brichet, E. A geo sub-bottom sulfide samples at the TAG active mound. In Proceedings of the Ocean Drilling Program-Scientific Results, Charleston, SC, USA, 8 January 1997; Herzig, P.M., Humphris, S.E., Miller, D.J., Zierenberg, R.A., Eds.; Texas A&M University: College Station, TX, USA, 2001; Volume 158, pp. 111–118. [CrossRef]
22. Murton, B.J. *Shipboard Scientific Party Cruise Report: Expedition JC 138: 29th June–8th August 2016, Mid Atlantic Ridge, 26°8.38′ N; 44°49.92′ W*; National Oceanography Centre Southampton: Southampton, UK; p. 285. Available online: https://www.bodc.ac.uk/resources/inventories/cruise_inventory/reports/jc138.pdf. (accessed on 18 July 2018).
23. Keith, M.; Haase, K.M.; Schwarz-Schampera, U.; Klemd, R.; Petersen, S.; Bach, W. Effects of temperature, sulfur, and oxygen fugacity on the composition of sphalerite from submarine hydrothermal vents. *Geology* **2014**, *42*, 699–702. [CrossRef]
24. Scott, S.D.; Barnes, H.L. Sphalerite geothermometry and geobarometry. *Econ. Geol.* **1971**, *66*, 653–669. [CrossRef]
25. Hannington, M.D.; De Ronde, C.E.J.; Petersen, S. Sea-Floor Tectonics and Submarine Hydrothermal Systems. In *Economic Geology One Hundredth Anniversary Volume*; Hedenquist, J.W., Thompson, J.F.H., Goldfarb, R.J., Richards, J.P., Eds.; Society of Economic Geologists (SEG): Littleton, CO, USA, 2005; pp. 111–141. ISBN 978-1-887483-01-8.
26. Large, R.R. Australian volcanic-hosted massive sulfide deposits: Features, styles and genetic models. *Econ. Geol.* **1992**, *87*, 471–510. [CrossRef]
27. Sugaki, A.; Shima, H.; Kitakaze, A.; Harada, H. Isothermal phase relations in the system Cu-Fe-S under hydrothermal conditions at 350 degrees C and 300 degrees C. *Econ. Geol.* **1975**, *4*, 806–823. [CrossRef]
28. Krasnov, S.G.; Cherkashev, G.A.; Stepanova, T.V.; Batuyev, B.N.; Krotov, A.G.; Malin, B.V.; Maslov, M.N.; Markov, V.F.; Poroshina, I.M.; Samovarov, M.S.; et al. Detailed geological studies of hydrothermal fields in the North Atlantic. In *Hydrothermal Vents and Processes*; Parson, L.M., Walker, C.L., Dixon, D.R., Eds.; The Geological Society: London, UK, 1995; Volume 87, pp. 43–64. ISBN 978-1897799253.
29. Butler, I.B.; Rickard, D. Framboidal pyrite formation via the oxidation of iron (II) monosulfide by hydrogen sulphide. *Geochim. Cosmochim. Acta* **2000**, *64*, 2665–2672. [CrossRef]
30. Wilkin, R.T.; Barnes, H.L. Formation processes of framboidal pyrite. *Geochim. Cosmochim. Acta* **1997**, *61*, 323–339. [CrossRef]
31. Murowchick, J.B.; Barnes, H.L. Marcasite precipitation from hydrothermal solutions. *Geochim. Cosmochim. Acta* **1986**, *50*, 2615–2659. [CrossRef]
32. Davis, A.S.; Clague, D.A.; Zierenberg, R.A.; Wheat, C.G.; Cousens, B.L. Sulfide formation related to changes in the hydrothermal system on Loihi seamount, Hawai'i following the seismic event in 1996. *Can. Miner.* **2003**, *41*, 457–472. [CrossRef]
33. Rimstidt, J.D. Gangue mineral transport and deposition. In *Geochemistry of Hydrothermal Ore Deposits*; Barnes, H.L., Ed.; John Wiley and Sons: New York, NY, USA, 1997; pp. 487–515. ISBN 978-0-471-57144-5.

34. Moh, G.H. Blue reaming covellite and its relations to phases in the sulfur rich portion of the copper-sulfur system at low temperatures. *Mineral. Soc. Jpn.* **1971**, *1*, 226–232.
35. Roseboom, E.H. An investigation of the system Cu-S and some natural copper sulfides between 25° and 700°C. *Econ. Geol.* **1966**, *61*, 641–672. [CrossRef]
36. Blount, C.N.; Dickson, F.W. The solubility of anhydrite ($CaSO_4$) in NaCl-H_2O from 100 to 450 °C and 1 to 1000 bars. *Geochim. Cosmochim. Acta* **1969**, *33*, 227–245. [CrossRef]
37. Tivey, M.K. Modeling chimney growth and associated fluid flow at seafloor hydrothermal vent sites. In *Seafloor Hydrothermal Systems: Physical, Chemical, Biological and Geological Interactions*; Humphris, S.E., Zierenberg, R.A., Mullineaux, L.S., Thomson, R.E., Eds.; American Geophysical Union: Washington, DC, USA, 1995; Volume 91, pp. 158–177. [CrossRef]
38. Edmond, J.M.; Campbell, A.C.; Palmer, M.R.; Klinkhammer, G.P.; German, C.R.; Edmonds, H.N.; Elderfield, H.; Thompson, G.; Rona, P.A. Time series studies of vent fluids from the TAG and MARK sites (1986,1990) Mid-Atlantic Ridge: A new solution chemistry model and mechanism for Cu/Zn zonation in massive sulfide orebodies. In *Hydrothermal Vents and Processes*; Parson, L.M., Walker, C.L., Dixon, D.R., Eds.; The Geological Society: London, UK, 1995; Volume 87, pp. 77–86. ISBN 978-1897799253.
39. Koski, R.A.; German, C.R.; Hein, J.R. Fate of hydrothermal products from Mid-ocean Ridge Hydrothermal Systems—Near-field to global perspectives. In *Energy and Mass Transfer in Marine Hydrothermal Systems*; Halbach, P.E., Tunnicliffe, V., Hein, J.R., Eds.; Dahlem University Press: Berlin, Germany, 2003; pp. 317–335. ISBN 978-3934504127.
40. Wohlgemuth-Ueberwasser, C.C.; Viljoen, F.; Petersen, S.; Vorster, C. Distribution and solubility limits of trace elements in hydrothermal black smoker sulfides: An in-situ LA-ICP-MS study. *Geochim. Cosmochim. Acta* **2015**, *159*, 16–41. [CrossRef]